



# Self-organization as a mechanism of resilience in dryland ecosystems

Sonia Kéfi<sup>a,b,c,1</sup> , Alexandre Génin<sup>a,d,e</sup> , Angeles Garcia-Mayor<sup>d,f</sup>, Emilio Guirado<sup>g</sup> , Juliano S. Cabral<sup>g,h</sup> , Miguel Berdugo<sup>f</sup> , Josquin Guerber<sup>a,i</sup> , Ricard Solé<sup>b,j,k</sup>, and Fernando T. Maestre<sup>g,l</sup>

Edited by Alan Hastings, University of California Davis, Davis, CA; received March 29, 2023; accepted December 11, 2023

Self-organized spatial patterns are a common feature of complex systems, ranging from microbial communities to mussel beds and drylands. While the theoretical implications of these patterns for ecosystem-level processes, such as functioning and resilience, have been extensively studied, empirical evidence remains scarce. To address this gap, we analyzed global drylands along an aridity gradient using remote sensing, field data, and modeling. We found that the spatial structure of the vegetation strengthens as aridity increases, which is associated with the maintenance of a high level of soil multifunctionality, even as aridity levels rise up to a certain threshold. The combination of these results with those of two individual-based models indicate that self-organized vegetation patterns not only form in response to stressful environmental conditions but also provide drylands with the ability to adapt to changing conditions while maintaining their functioning, an adaptive capacity which is lost in degraded ecosystems. Self-organization thereby plays a vital role in enhancing the resilience of drylands. Overall, our findings contribute to a deeper understanding of the relationship between spatial vegetation patterns and dryland resilience. They also represent a significant step forward in the development of indicators for ecosystem resilience, which are critical tools for managing and preserving these valuable ecosystems in a warmer and more arid world.

drylands | self-organization | spatial patterns | desertification

Abrupt, irreversible changes in ecosystems are a serious concern given the forecasts for future environmental changes and their expected pace (1). Urgently needed tools are being developed to characterize and anticipate shifts in ecosystem functioning and stability. While many of these tools rely on analyzing temporal changes in ecosystem properties, the spatial structure of some ecosystems can also teach us about the way these ecosystems cope with stressors such as changes in climate (2–5). Indeed, interactions between species and their environment can generate emergent spatial patterns even in the absence of underlying heterogeneity, referred to as “self-organized” patterns (3, 6, 7). Drylands are one of the textbook examples of ecosystems showing such patterns, as their vegetation cover presents a striking spatial structure that displays well-defined statistical properties across large spatial scales (2, 8–10). One of the most commonly hypothesized underlying mechanisms is that, in the harsh environmental conditions of drylands, established vegetation improves the local environmental conditions and alters the redistribution of resources—in particular water—from bare areas to vegetation patches, which promotes the spatial aggregation of plants (3, 7, 8, 11–14).

Theoretical studies have long suggested that self-organized spatial patterns could increase overall ecosystem function and resilience (3, 4, 6, 11, 13). Indeed, the capacity of drylands to spatially self-organize is predicted to allow them to maintain a higher productivity than what would be expected in the absence of spatial structure (3, 7, 11, 13). These self-organized patterns may change with environmental conditions, such as water shortage, giving drylands the ability to adapt and maintain productivity by adjusting their spatial structure (3, 11, 13). This is expected to lead to relatively stable levels of ecosystem functioning despite increasing stress, allowed by changes in spatial patterns. However, empirical support for this hypothesis is still elusive. Furthermore, spatial vegetation patterns can also hold the key to another generic phenomenon of interest: critical slowing down (5). Indeed, theoretical models have shown that self-organized spatial patterns could also be used as indicators of resilience loss because they reflect the speed required by the system to recover from perturbations (15): as a dynamical system approaches a point at which its stability changes drastically, it takes a longer time to recover from small perturbations, which leaves traces both in the temporal and in the spatial dynamics of the system (15, 16). As a consequence, spatial structure is expected to show increasing variance and auto-correlation

## Significance

The spatial structure of vegetation in dryland ecosystems has long fascinated scientists due to its striking appearance. Through a combination of global field surveys, mathematical models, and remote sensing, we show that the mechanisms responsible for these patterns enable healthy dryland ecosystems to adapt to changing environmental conditions, including water shortages, by adjusting their spatial structure. Conversely, degraded ecosystems do not have this ability. Our findings underscore the critical role of spatial pattern formation in promoting resilience in dryland ecosystems. Moreover, these spatial patterns could serve as valuable indicators of ecosystem health under a changing climate, opening important perspectives for future research in this field.

Author contributions: S.K. designed research; S.K. and A.G. performed research; S.K., A.G., and J.G. analyzed data; F.T.M. collected the data; and S.K., A.G., A.G.-M., E.G., J.S.C., M.B., R.S., and F.T.M. wrote the paper.

The authors declare no competing interest.

This article is a PNAS Direct Submission.

Copyright © 2024 the Author(s). Published by PNAS. This article is distributed under [Creative Commons Attribution-NonCommercial-NoDerivatives License 4.0 \(CC BY-NC-ND\)](https://creativecommons.org/licenses/by-nc-nd/4.0/).

Although PNAS asks authors to adhere to United Nations naming conventions for maps (<https://www.un.org/geospatial/mapsgeo>), our policy is to publish maps as provided by the authors.

<sup>1</sup>To whom correspondence may be addressed. Email: [sonia.kefi@umontpellier.fr](mailto:sonia.kefi@umontpellier.fr).

This article contains supporting information online at <https://www.pnas.org/lookup/suppl/doi:10.1073/pnas.2305153121/-/DCSupplemental>.

Published February 1, 2024.

(referred to as “spatial early warnings”) as the ecosystem loses resilience (meaning as its recovery capacity decreases) (5, 17).

Previous empirical studies have analyzed changes in vegetation patterns along local gradients (2, 18, 19) or in specific aspects of the vegetation patches across large spatial scales (9, 10, 20). However, building a robust predictive framework for dryland ecosystems requires going a step further by confronting theoretical predictions from mechanistic models to empirical observations covering large geographical scales and stress gradients. Doing so is essential to validate with confidence the causality of theoretical predictions about vegetation spatial patterns, their importance in maintaining dryland ecosystem resilience, and to evaluate whether and how spatial patterns can be used as early warning signals for the onset of desertification and abrupt ecosystem shifts (2–5, 11).

Here, we provide unique empirical support for the hypothesis that changes in the spatial structure of vegetation lead to relatively stable levels of dryland ecosystem functioning despite increasing stress. We used a global dataset of 115 dryland sites (Fig. 1), for which field and remotely sensed data about their soil and vegetation features were gathered (21). After classifying the high resolution remote sensing images of our dataset into presence/absence of vegetation, we estimated vegetation cover and quantified its spatial

structure using relevant spatial metrics based on theoretical studies (5): patch-based metrics (number and size of the vegetation patches), hydrological connectivity (connectivity of the bare-soil area reflecting the overall potential of the landscape to redistribute or lose resources by runoff), and spatial early warnings (quantifying the resilience of the ecosystem) (*Materials and Methods*). At the global scales, we directly compared the observed trends in these metrics along an aridity gradient to those produced by two different theoretical models previously used to investigate the emergence of spatial patterns in drylands (8, 13). These models describe the spatiotemporal dynamics of the vegetation assuming local facilitation (i.e., plants improve their local environment thereby facilitating the recruitment of others in their direct neighborhood) and global competition for limiting resources such as water (*Materials and Methods*).

## Results

A two-dimensional clustering analysis of the vegetation cover and soil multifunctionality (i.e., an index derived from field measurements of carbon, nitrogen and phosphorus in the soil) of the field sites surveyed revealed that our dryland sites could be split into two distinct groups of relatively “healthier” (those with relatively high

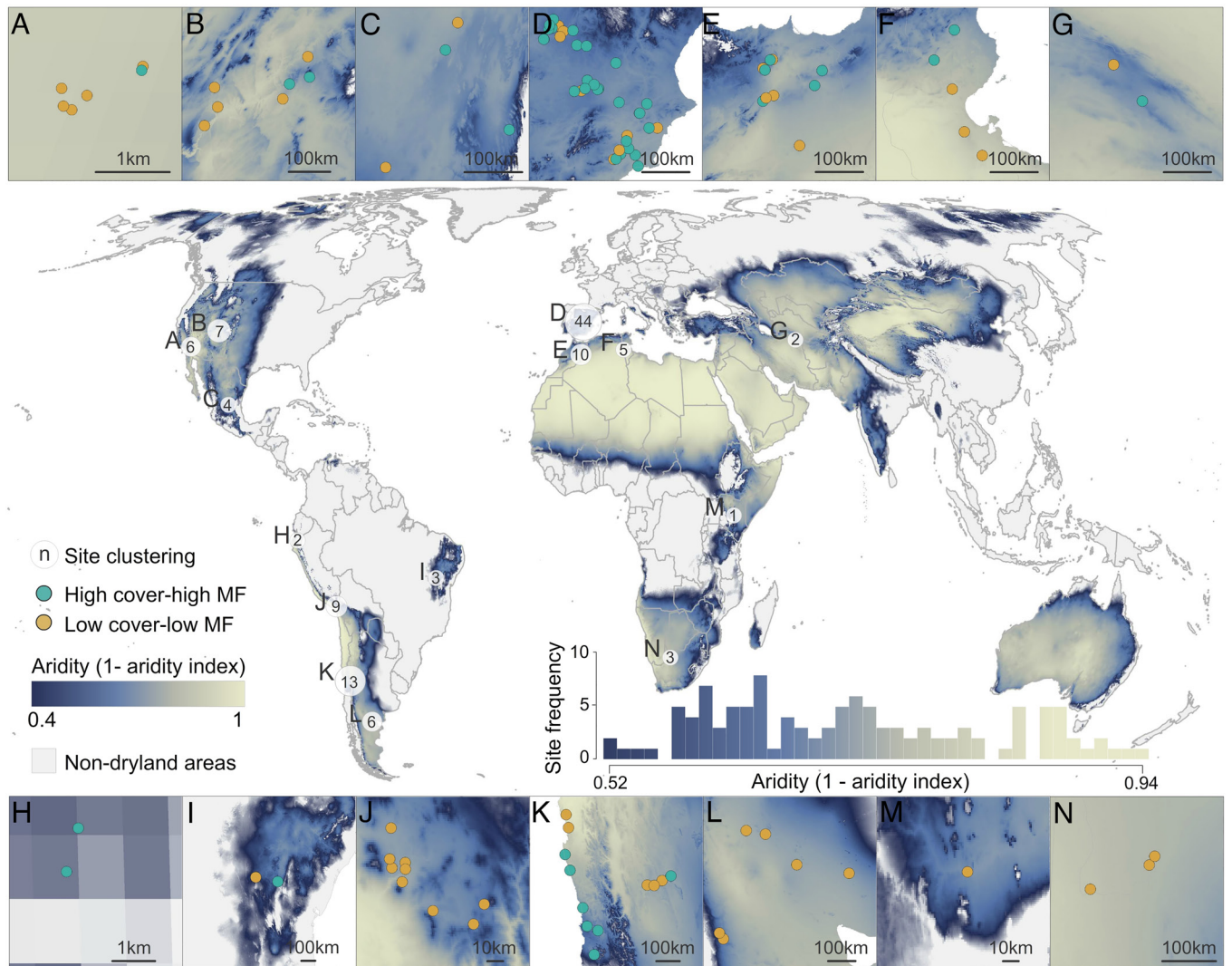


**Fig. 1.** Location of the 115 plots in the global drylands dataset used. Surveyed sites are colored in green for the healthier sites (high vegetation cover—high soil multifunctionality, MF) and yellow for the degraded sites (low vegetation cover—low multifunctionality, MF). Numbers reflect the number of sites in a given geographical area (characterized by the letters A–N), for which a corresponding zoom can be found in the panels above and below the map.

cover and soil multifunctionality) vs. “degraded” sites (those with relatively low cover and soil multifunctionality; Fig. 2 and *SI Appendix*, Fig. S11). These two groups of sites differ significantly in all spatial metrics measured on vegetation cover but spatial autocorrelation (i.e., *Spectral Density Ratio*; Fig. 3). Compared to degraded sites, healthier sites have larger patches, less connected bare areas (i.e., lower *flowlength*), and an overall less fragmented vegetation cover (i.e., steeper slope of the patch size distribution) (Figs. 3 and 4).

Across all the sites surveyed, the fragmentation of the vegetation cover increases with aridity, driving changes in patch-based metrics that match the expectation from theoretical models (Fig. 5 *A* and *B* and *SI Appendix*, Fig. S7). As environmental conditions become more stressful, the loss and fragmentation of vegetation cover led to a change in the shape of the patch size distribution (2, 22, 23) and to an increase in the connectivity of bare-soil areas, as shown by increased values of *flowlength* (24). These trends need to be compared to the expected changes caused by the loss of vegetation cover for random spatial structure, hereafter called null model (*Material and Methods*), to assess whether the observed changes can be purely explained by a decrease in cover under more arid conditions. We found that the observed breakdown of the patch size distribution in field sites is weaker than expected in the null model (compare the colored and the gray points for patch-based metrics in Fig. 5 *A* and *B* and *SI Appendix*, Fig. S7 and S2). This means that vegetation in drylands is more spatially structured than expected and is growingly so as aridity increases.

Separate analyses of healthier and degraded sites revealed that the relative increase in spatial structure with aridity mainly occurs for the healthier sites (Fig. 5 *C*, *Left*). These results indicate that healthier sites thereby keep adapting their spatial structure as environmental conditions worsen. For all patch-based metrics evaluated, the deviation from randomness increases with aridity. This result suggests an increasing role of mechanisms enhancing the spatial aggregation of plants along the aridity gradient (8). Indeed, in the absence of such processes, spatial structure emerges in the two theoretical models but is not different from a null expectation (*SI Appendix*, Figs. S8 and S9). Possible underlying mechanisms to explain our results include positive plant interactions (7), eco-hydrological feedbacks driving resource (especially water) redistribution in the landscape (24, 25), exogenous phenomena [e.g., spatial structure in soil moisture (26)], or a combination of these mechanisms. The nature of our survey and analyses does not allow us to strictly conclude on the presence and importance of such mechanisms. However, the fact that bare-soil connectivity increases with aridity in the healthier group of sites—as shown by a significant increase in *flowlength*—and the fact that it does so more than in the null model (Fig. 5 *C*, *Left*), suggests that at least water distribution within the ecosystem plays a role (25). Indeed, an increase in *flowlength* means that vegetation patches receive resources (e.g., water, nutrients) from a larger bare-soil area than would be expected with a randomized spatial structure.

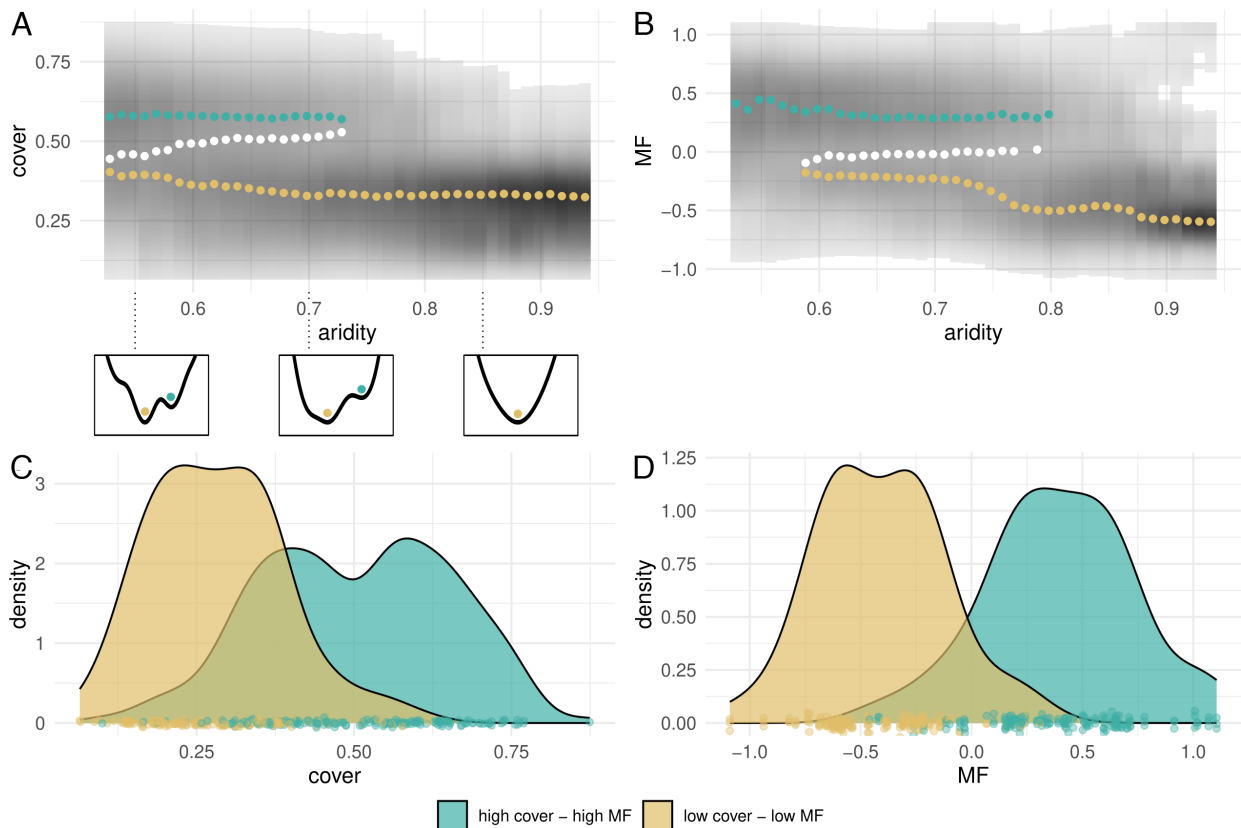


**Fig. 2.** Dryland ecosystems were categorized into two groups using vegetation cover and soil multifunctionality data. (A) Cover and (B) soil multifunctionality (MF) along aridity for all 115 sites colored by the two groups: healthier (high cover–high soil multifunctionality values; in green) and degraded (low cover–low soil multifunctionality values; in yellow). Aridity was calculated as:  $1 - \text{Aridity Index (AI)} = \text{precipitation/potential evapotranspiration}$ , so that higher values indicate drier conditions. Colored points are the maxima of reconstructed stability landscapes based on potential analysis (i.e., possible attractors), while the white ones are the minima (*Materials and Methods*). Small panels below A display examples of stability landscapes for aridity values 0.55, 0.7, and 0.85, where valleys in the landscape are the colored points of panel A and the hills the white points (*Materials and Methods*). (C and D) Densities of sites for each of the two groups for cover (C) and soil multifunctionality data (D).

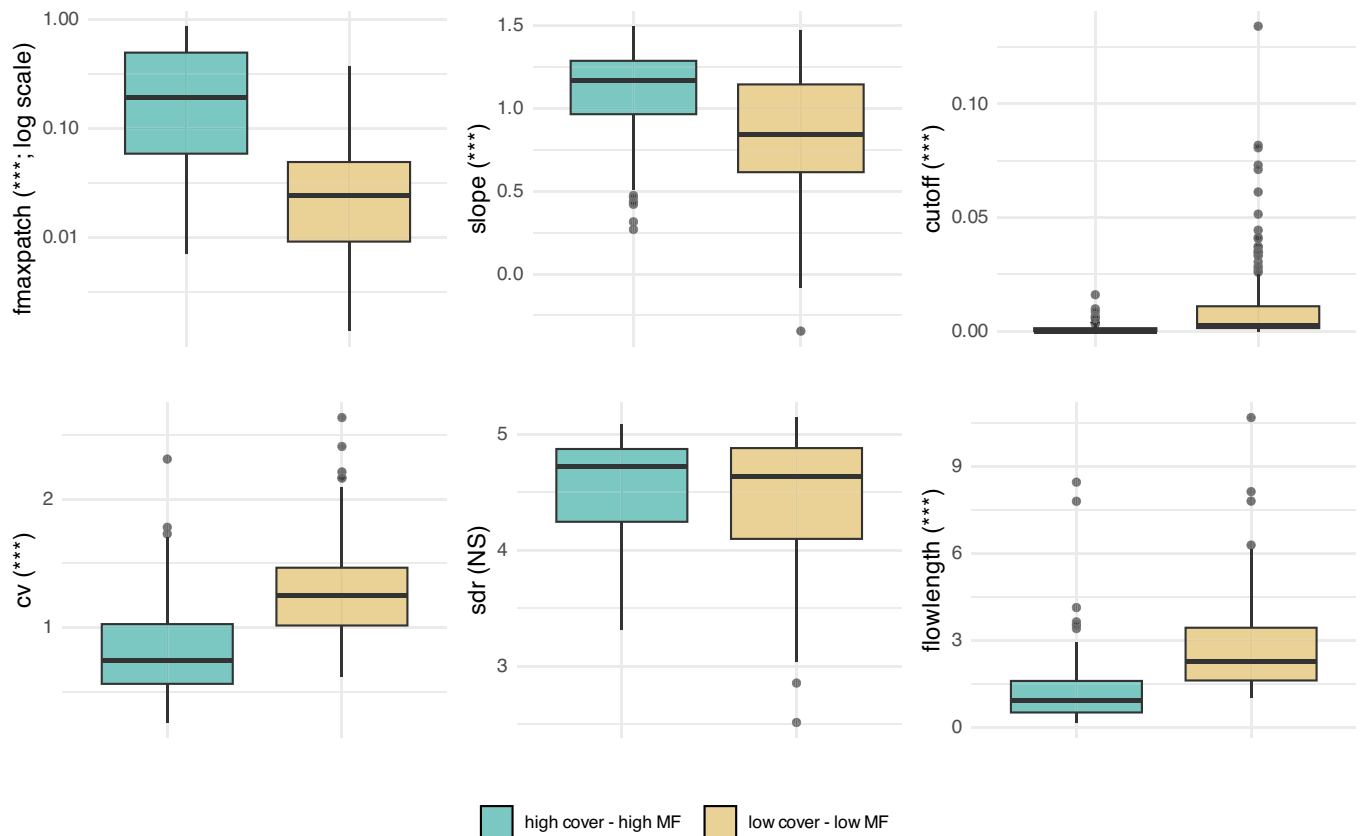


**Fig. 3.** Differences in the spatial structure of the vegetation cover between healthier (high cover, high soil multifunctionality) and degraded (low cover–low soil multifunctionality) drylands. The spatial metrics are the proportion of the image covered by the largest vegetation patch [*fmaxpatch*, (largest patch/image size), with the y axis on a log scale], the slope of the patch size distribution, the cutoff of the patch size distribution, spatial variance, the Spatial Density Ratio (*sdr*), and the bare soil connectivity (*flowlength*). For all metrics but *sdr*, the differences between the two groups are significant (*SI Appendix*, Table S3).

In the degraded sites, trends in patch-based and in hydrological connectivity metrics break down along the aridity gradient: All trends are weaker than those in the healthier group of sites—several being not significant—and they are closer to the null expectation (Fig. 5 *C*, *Right*). These findings indicate that the ability of the sites to undergo spatial reorganization under stress diminishes, associated with a decline in functioning. This is evident from the significant decrease in soil multifunctionality observed for these sites in response to increasing aridity ( $P = 1.2 \times 10^{-5}$ , *SI Appendix*, Fig. S13).

For the healthier sites, since only spatial variance changes significantly but not spatial autocorrelation, the spatial early warnings suggest no sign of resilience loss as aridity increases (Fig. 5 *C*, *Left*). This is consistent with those sites showing limited signs of “suffering” from increasing aridity: Cover decreases significantly with aridity because of constraints in water availability ( $P = 3.7 \times 10^{-7}$ , *SI Appendix*, Fig. S13), but functioning is maintained through the spatial reorganization of the cover (no significant decrease in soil multifunctionality with aridity;  $P = 0.8$ , *SI Appendix*, Fig. S13). However, in the degraded group of sites, spatial early warnings do suggest a loss of resilience as aridity increases (Fig. 5 *C*, *Right*), which probably reflects an overall physiological threshold of the vegetation at the end of the aridity gradient (27).

## Discussion

Our results, using a thorough evaluation of multiple spatial metrics—which reflect different facets of ecosystem resilience—provide unique insights on how drylands cope with abiotic stress and

how their spatial structure contributes to improve their resilience to increased aridity conditions. Despite the large environmental variability found across the different field sites studied, the overall consistency of the observed changes in spatial metrics along an aridity gradient with theoretical predictions is remarkable.

In this work, we have considered two different minimal models of dryland dynamics that share local facilitation and non-local (long-range) effects as the two necessary drivers that generate self-organized patterns with fat-tailed cluster distributions. Despite their differences, these two models successfully matched the repertoire of spatial patterns found in our data (2, 8, 22). This supports the idea of universality as defined in physics: Macroscopic patterns in far-from-equilibrium systems can be accounted for from minimal interaction rules (28–30). In other words, simple mechanistic models can provide reliable predictions beyond the specific, low-scale details. It is noteworthy that other types of drylands than the ones studied here, such as semiarid savannas, have been found to exhibit a different type of behavior: Available data (31) and a different class of stochastic models (26) indicate that their spatial patterns show broadly similar features as those found in our data but are caused by exogenous phenomena associated with the formation of soil moisture islands that determine the spatiotemporal dynamics of tree clusters (26). In these latter systems, we do not expect the same trends in spatial metrics as those found here along an aridity gradient.

Disentangling the mechanisms driving the self-organization and stability of drylands may require metrics grounded in empirically proven mechanisms, such as eco-hydrological feedbacks evaluated in the field by the metric *flowlength*. The fact that bare-soil

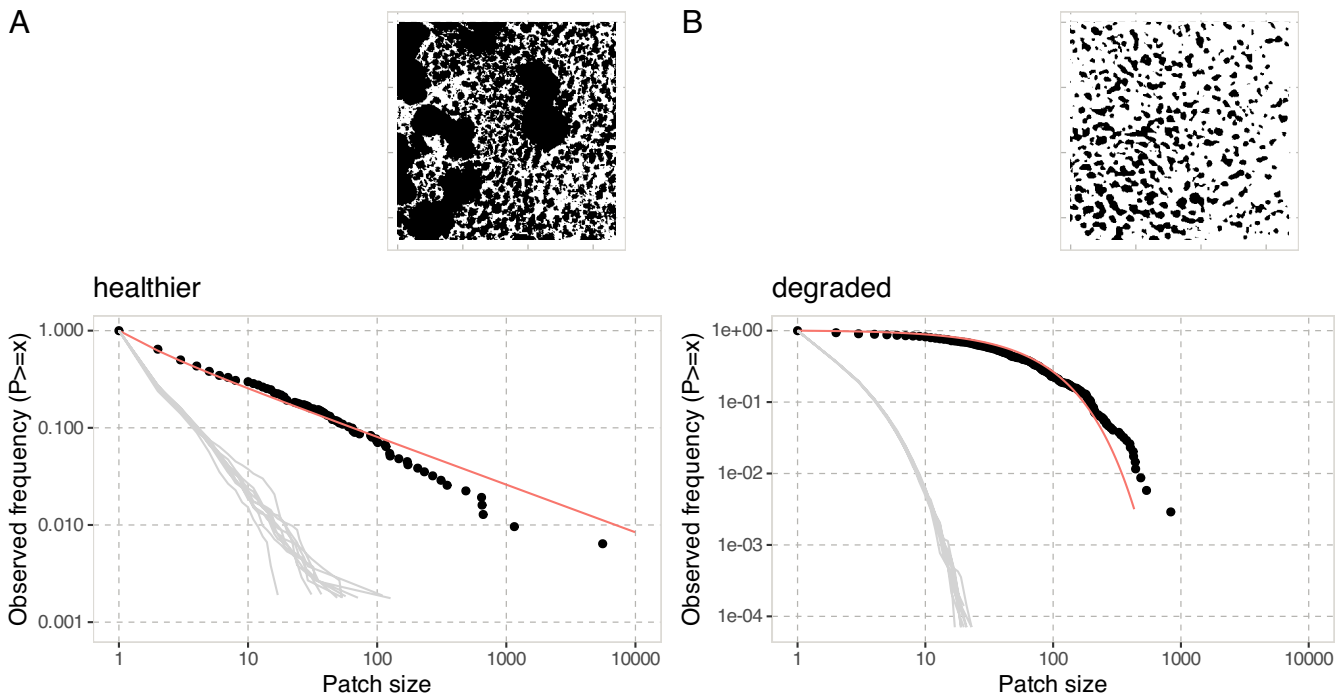


**Fig. 4.** Examples of patch size distributions of a healthier site (A) and a degraded one (B). Sites are two grasslands (images 148-b and 192-c of the dataset). Graphs display the fraction of patches larger than a certain size. Black points are observations from the image and gray curves are random expectations (based on 10 randomizations of the image). The red curve is the best fit. Snapshots on the *Top Right* are the images (black reflects vegetation).

connectivity increases with aridity in the healthier group of sites and that it does so more than in the null model (Fig. 5 C, *Left*) point toward the fact that such mechanism could include resource distribution within the ecosystem (25). The consequences of this process on ecosystem stability are thought to arise from two main eco-hydrological feedbacks of opposite signs in drylands (25). At a local (patch) scale, an increase in bare-soil connectivity leads to a redistribution of resources from bare areas to vegetation patches; this self-regulating (negative) feedback is overall stabilizing. At the ecosystem scale, bare-soil connectivity increases runoff and therefore the potential losses of resources from the ecosystem; this reinforcing (positive) feedback has been shown to be destabilizing (25). The balance between these two feedback loops determines the hydrological response of the ecosystem in terms of whether connectivity is overall stabilizing or destabilizing (25) and thus the ecosystem ability to maintain itself in a productive state or degrade into a more barren, less productive state. In the healthier group of sites, the trends in spatial metrics found are consistent with the dominance of a stabilizing feedback: an increase in bare-soil connectivity leads to more resource redistribution from bare to vegetation areas, which leads to more vegetation patchiness (i.e., deviation from random structure) and a further increase in connectivity, which contributes to the overall higher functioning (i.e., higher soil multifunctionality) and cover of these sites compared to the degraded sites. Conversely, the stabilizing feedback appears weaker in the degraded group of sites. Our findings thereby empirically support one key prediction of theoretical models, namely that resource redistribution from bare to vegetated patches, driven by bare soil connectivity, is a fundamental mechanism that determines the emergent spatial structure of arid ecosystems (14, 24, 25).

Here, our analyses identified two alternative ways in which global drylands respond to increasing abiotic stress through self-organization: one in which the vegetation patterns are building resilience but also another in which this ability of the ecosystem is lost. In the first case, i.e., in self-organized ecosystems,

spatial structure reinforces itself with increasing aridity (i.e., the deviation from a random structure increases). These changes in spatial structure, which are associated with maintaining soil multifunctionality, help to mitigate the increased stress despite a decrease in cover by allowing the ecosystem to retain enough water and maintain its overall functioning, which is consistent with the idea that spatial self-organization is a mechanism of resilience at the ecosystem scale (4). Importantly, we also found that failure to perform such changes in spatial structure, and thereby retain resources, in degraded sites leads to a loss in functioning and resilience. Our results empirically highlight the essential role of spatial patterns, and more specifically of the self-organization process, for dryland functioning and resilience.

It is noteworthy that if vegetation patchiness allows the maintenance of cover and functioning for a large range of aridity values, it only does so below an aridity threshold of 0.8 (Fig. 2). Indeed, there are no high cover, high soil multifunctionality sites above an aridity level of 0.8. Therefore, if aridity increases beyond that threshold in some of the sites of the healthier group, we expect them to eventually shift to the degraded group of sites, thereby losing their cover and soil multifunctionality. We expect sites to shift because there are only two (or maybe 3; see *SI Appendix, Fig. S11*) groups of sites globally, meaning that there is a limited number of states for dryland ecosystems to be in. This aridity threshold of 0.8 corresponds to a known documented point at which drylands exhibit a dramatic loss of vegetation cover accompanied by a decrease in species richness as well as a change in plant leaf strategy from stress tolerance to stress avoidance (27).

Recent studies have suggested that spatial self-organization does not only contribute to increase ecosystem resilience but can also allow them to evade tipping points (4). Interestingly, our results imply that we do not have evidence that the ecosystems studied here are evading a tipping point to desertification thanks to pattern formation [as suggested for regular vegetation patterns (4)]. Indeed, the self-organization process seems to only be effective in

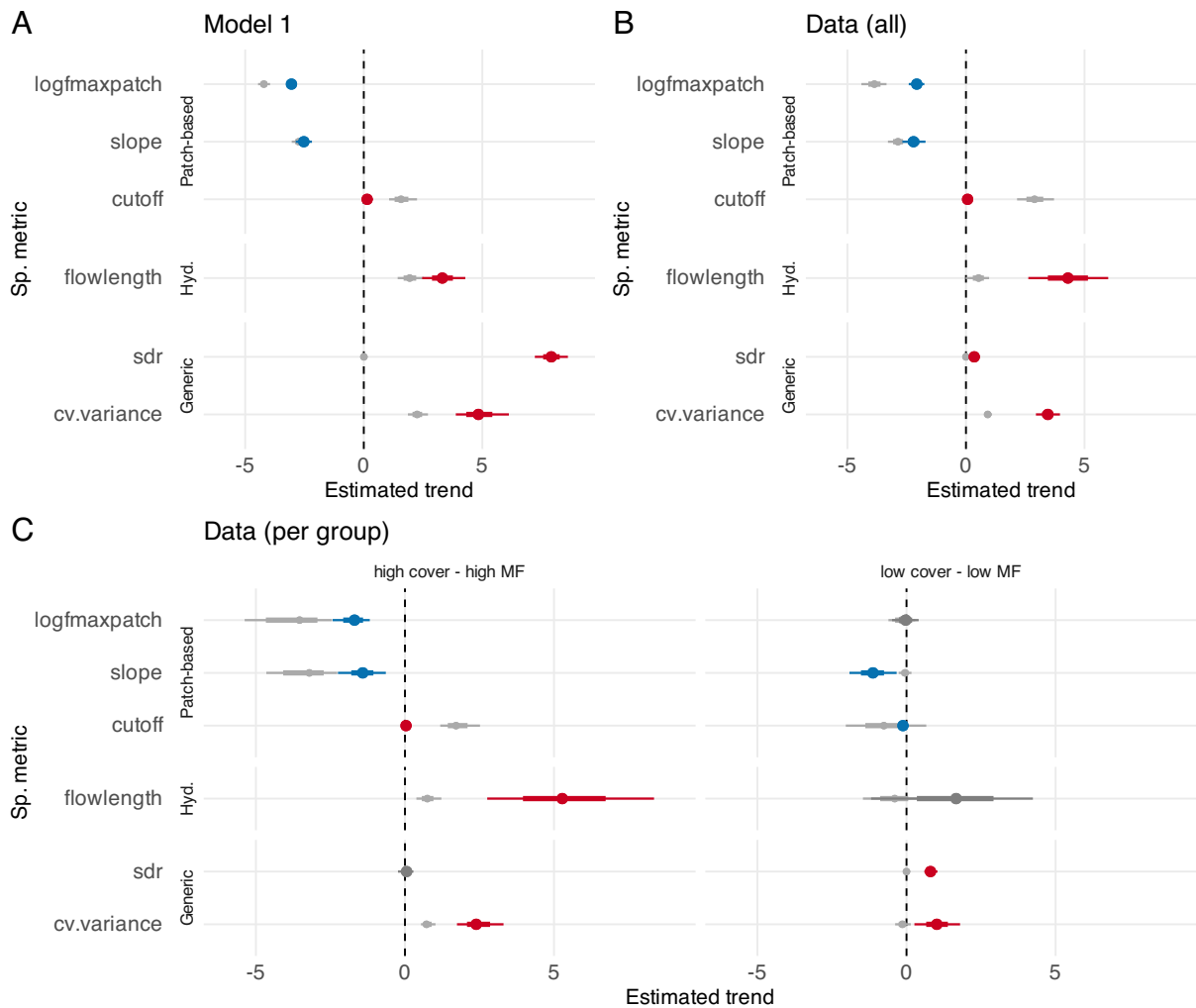


**Fig. 5.** Estimated slope of the trends in spatial metrics along the aridity gradient evaluated in the model (A), in all the field sites of the dataset (B) and in the two groups of sites separately (C; healthier sites on the left and degraded sites on the right; MF stands for soil multifunctionality). Points reflect the value of the slope of the spatial metrics with aridity. Significant positive and negative slopes are in red and blue, respectively. Observed slopes are in color, while expected trends of randomized landscapes (keeping cover constant but with reshuffled image pixels) are in gray. See legend of Fig. 3 and *Materials and Methods* for definitions of the spatial metrics. See *SI Appendix D* for a discussion of the difference in the slopes of SDR in the model and in the data.

healthier sites and up to a threshold level in aridity. It is however noteworthy that we are here comparing different ecosystems in space and not following the temporal dynamics of a given ecosystem in time, which could draw a different picture of an ecosystem response to increasing stress. Learning about whether the sites studied are approaching a tipping point or not would require temporal data, a matter for future research.

The fact that the observed changes in spatial metrics along the aridity gradient in healthier sites are consistent with theoretical predictions is a crucial step in the development of reliable indicators of desertification in drylands. Theoretical studies have suggested for a long time that the spatial structure of vegetation patterns in drylands could be used to inform about the stress level experienced by dryland ecosystems (2, 3, 11). Patch-based and hydrological metrics inform about the ability of the ecosystem to adapt to increasing stress through self-organization [i.e., they inform about “ecological resilience” *sensu* C.S. Holling (32)], while spatial early warnings inform about the recovery of the system after a perturbation (i.e., “engineering resilience”). Both types of metrics provide different but complementary information about the ecosystem’s ability to respond to increasing stress (*SI Appendix, Fig. S4*). Finding consistent trends in spatial metrics in data and

models is a significant progress, but a knowledge gap still remains before we can build reliable spatial indicators of ecosystem degradation, in particular, indicators which can allow us to determine which ecosystems are more fragile than others. In particular, one of the issues is that we need to get a better understanding of how different mechanisms, e.g., due to the external pressures applied on ecosystems, can affect the spatial patterns and possibly blur the signals observed here (23, 33–36). Explicit data on land use intensity are needed to be able to address that concern.

By combining remote sensing, field data, and model simulations, our study contributes to building a more robust framework to assess dryland degradation status. Our findings are relevant to help identifying which drylands are more fragile, and, therefore, where efforts to preserve them and prevent their degradation should be focused on. They also highlight the need for a system-level, spatial picture of dryland vegetation, since spatial structure is both a driver of increasing resilience and an early warning indicator of future ecosystem changes. Such efforts are instrumental to avoid declines in ecosystem functioning that will reduce the delivery of essential ecosystem services, forcing dryland inhabitants (which are already vulnerable) to either migrate or change their livelihood drastically in the near future.

## Materials and Methods

**Data.** The field dataset contains vegetation and soil data from 115 dryland ecosystems located in 13 countries (the data are described in detail in ref. 21). The sites used (Fig. 1) differ widely in their abiotic (elevation, temperature, and precipitation) and biotic (vegetation type, cover, and number of species) characteristics (see database in figshare: <https://figshare.com/s/3db3640a61ebc975bcd>).

At each site, a 30 m × 30 m plot representative of the vegetation present in that area was established in the field and plant cover was estimated using the line intercept method (see more details in ref. 21). Five soil cores (0 to 7 cm depth) were taken in areas devoid of perennial vegetation (to avoid implicit effects of vegetation cover within multifunctionality measurements) and 16 variables were measured related to the carbon (C; organic C, β-glucosidase activity, pentoses, hexoses, aromatic compounds, and phenols), nitrogen (N; nitrate, ammonium, total N, potential N transformation rate, amino acids and proteins), and phosphorus (P; Available P, phosphatase activity, inorganic P and total P) cycles. Variables are considered to be critical determinants of ecosystem functioning in drylands. They were used to calculate a soil multifunctionality index, multifunctionality, obtained as the average Z-score across these variables (21). High values of soil multifunctionality have been associated with more functional ecosystems (20).

Values of the aridity index (AI, precipitation/potential evapotranspiration) were obtained from Zomer et al. (37), who used the data interpolations provided by Worldclim (38). To facilitate the interpretation of the results, we calculated the aridity level of each site as  $1 - AI$  (39). Indeed, as formulated, AI decreases when aridity increases, which is not intuitive; Using  $1 - AI$  instead of AI solves this issue as our proxy of aridity increases as aridity does (so higher values of this aridity level indicate drier conditions), which makes our results easier to understand.

For each study site, remote sensing data were obtained from ref. 20. The data consist in Google EarthTM (<https://earth.google.com/>) or VirtualEarthTM (<http://www.bing.com/maps>) images of sufficient quality to visually identify vegetation patches. For each field site, three 50 m × 50 m images were collected, one of them was centered on the 30 m × 30 m plot surveyed in the field, and the other two were located nearby, avoiding strong slopes and man-made structures like roads or buildings. Each image was transformed to identify vegetation vs bare soil pixels: A k-mean classification approach implemented in Matlab (The MathWorks Inc., MATLAB v. 7.5.0.342, R2007b) was used to partition the pixels in clusters of luminance intensity (using a monochromatic version of the image) (see ref. 20 for details). The transformed images contain information about the presence or absence of vegetation in each pixel.

As a surrogate of plant productivity, we used the normalized difference vegetation index (NDVI), which provides a global measure of the “greenness” of vegetation across the Earth’s landscapes and is positively linked with vegetation productivity (40). These data were retrieved from previous papers (20, 21) in which NDVI data for each plot were acquired using Landsat 5 TM and Landsat 7 ETM+, at a 30 m × 30 m resolution (<https://landsat.gscf.nasa.gov/>), i.e., at the resolution of the sampled plots. For each site, the mean annual NDVI for each year between 2000 and 2015 was calculated and then averaged for the entire period.

**Characterization of the Spatial Structure of the Vegetation.** We computed the spatial metrics on the matrices of presence-absence of vegetation inferred from the satellite images using the R package *spatialwarnings* (v3.0.3) (41, 42). Self-organized systems exhibit common changes in spatial structure as they approach a transition (5, 41). We calculated the generic spatial early warnings that are known to capture such changes (5, 41): spatial variance, near-neighbor correlation (*Moran’s I*), and spectral density ratio (*sdr*). Spatial variance, spatial correlation, and *sdr* are expected to increase as a dynamical system approaches a transition (a “bifurcation” point) (see *SI Appendix, Figs. S6 and S7* for expected trends along a stress gradient based on model simulations) (5, 17, 43, 44). Indeed, as an ecosystem is approaching a transition, neighboring cells are expected to become more similar (5). In the results, we did not display *Moran’s I* as it was highly correlated with *sdr* (correlation = 0.897).

For spatial variance, the matrices of presence-absence of vegetation were coarse-grained using  $4 \times 4$  submatrices as explained in refs. 5, 18, and 45. Note that this was not the case for spatial correlation which does not require coarse-graining. The principle of coarse-graining is that each matrix of dimension  $n \times n$  is transformed into nonoverlapping submatrices of size  $s \times s$  (with here  $s = 4$ ).

Each submatrix is then replaced by its average to obtain a smaller “coarse-grained matrix” of size  $c_g \times c_g$  where  $c_g = n/s$  (5).

For each matrix, two pixels are assumed to be part of the same vegetation patch if they are neighbors (one of the four nearest neighbors, i.e., von Neumann neighborhood). We thereby calculated the size of all the patches in a given matrix and extracted a number of “patch-based metrics.” We fitted a truncated power law to the patch size distribution of each matrix and recorded the exponent and the cutoff of the fit. We also recorded the fraction of the image covered by the largest patch using  $\log_{10}(\text{largest patch}/\text{image size})$ , where “image size” is the number of pixels (2, 5, 20, 22).

We calculated *flowlength*, a metric that measures the potential hydrological connectivity of runoff-source areas (e.g., bare soil) according to the vegetation cover, its spatial structure and the topography (14). *Flowlength* is defined as the average length of all the potential runoff pathways in the plot. Thus, a higher value of *flowlength* indicates a higher hydrological connectivity of runoff source areas. *Flowlength* has been suggested to be an indicator of dryland functional status by assessing potential water and soil losses in patchy landscapes (14, 24). See *SI Appendix, section B and Fig. S3* for additional information about *flowlength* calculations.

To estimate whether the spatial metrics for each plot differ from what would be expected based on the amount of cover, null expectations for the values of each of the spatial metric were obtained by reshuffling the pixels of the transformed matrices 199 times (5, 18, 41). The number 199 is estimated to be sufficient in this case because subsequent analyses only depended on the means of the null distributions created. The reshuffling process removes any spatial structure from the original data while keeping the vegetation cover fixed. The same spatial metrics were then calculated on the reshuffled matrices. Note that this works well in the model, where each pixel is assumed to be a plant, but in the images, depending on the plant species, a pixel can contain many individuals or a plant (tree) can be composed of many pixels.

Each of these metrics is quantified on the three matrices obtained for each field site (i.e., 345 values), except for *flowlength* which could only be measured on the plot among the three that was centered on the field plot (i.e., 115 values) since the slope of the field site is required to calculate *flowlength* and that information was only available for the plots sampled in the field.

**Clustering Analysis: Splitting Sites in Groups.** Clustering analyses were performed to see whether the dataset could be split in different groups of sites and, if so, in how many groups. We combined multiple clustering methods to build a consensus on the number of groups in the dataset as clustering results are sensible to the chosen method and the underlying assumptions. We started by clustering the distributions of vegetation cover and multifunctionality values in our dataset (i.e., two-dimensional clustering) using hierarchical clustering (*hclust*) based on a Euclidean distance matrix and a Ward distance, which is appropriate for globular clusters [using the *stats* package included in R v.4.2.0 (42)]. Inspecting the resulting tree (*SI Appendix, Fig. S11*) suggested that the dataset could be well-described by either two or three groups, which was confirmed by the result of a permutation-based analysis carried out using the function *simprof* in the *clustsig* R package v1.1 (42, 46), suggesting three significant groups. We further investigated this pattern based on a Gaussian mixture approach, using the best number of clusters based on the Bayesian Information Criterion (BIC). This was done using the *mclust* R package v6.0.0 in R (42, 47). This latter approach suggested the split of the dataset into two groups for all but one type of cluster shape, and in this specific case, only a small increase ( $<2$ ) in BIC was found by going from two to three groups (*SI Appendix, Fig. S11*). We thus considered the consensus classification into two groups as the most relevant to characterize the distribution of cover and multifunctionality in our dataset but provide all analyses for three groups in *SI Appendix, Figs. S16–S19*. We used the two groups predicted by the original hierarchical clustering (*SI Appendix, Fig. S11*), but those were in very close agreement (14 sites out of 345 are classified differently, 4%) with the clustering based on the Gaussian mixture approach. We refer to these two groups of sites as healthier (high cover–high soil multifunctionality) and degraded (low cover–low soil multifunctionality).

**Identification of Potential Stable States.** We used a density-based approach to detect dominant modes, which potentially reflect alternative states of the ecosystem, along the aridity gradient evaluated (48–50). This approach is based on

the relationship between the empirical distribution of a set observations of a dynamical system and its potential. Assuming the following dynamical system with a single state variable  $z$  and dynamics defined by a potential  $U$  (i.e.,  $dU/dz = -dz/dt$ ) along with a Wiener process  $dW$

$$dz = -U'(z)dt + \sigma dW,$$

where  $dW$  is a Wiener process and  $\sigma$  is the noise level, it can be shown (48–50) that there is a link between the empirical distribution of observations  $p_d$  and  $U$  as

$$U = \frac{-\sigma^2}{2} \log(p_d),$$

$p_d$  can be directly estimated from data using kernel density estimation. The above relationship formalizes the intuition that a dynamical system will tend to spend more time fluctuating around its stable equilibria and away from its unstable equilibria. It gives a direct way to estimate what are assumed to be stable and unstable equilibria: the local minima of the potential or stable equilibria correspond to the local maxima of the density, and the local maxima of the potential or unstable equilibria correspond to the local minima of the density.

To estimate  $p_d$  along a gradient of aridity, we used a rolling-window approach in which for each value of aridity, all observations of cover or multifunctionality are taken within a range of  $x - \text{wdw}/2$  and  $x + \text{wdw}/2$ , where  $x$  is the aridity value and  $\text{wdw}$  is the window size (here  $\text{wdw} = 0.15$ ). These are used to compute the distribution  $p_d$  and thus the hypothesized stable and unstable equilibria. Doing so for all values of aridity  $x$  provides a visualization of possible stable and unstable equilibria along the gradient and an estimation of the assumed potential. The distribution of states  $p_d$  was estimated using a gaussian kernel density estimator of width 0.3 (function density() in base R). This analysis was used for Fig. 2 A and B.

**Slope of Patterns along Aridity and other Statistical Analyses.** For the variables for which there was no replicate per site, i.e., 115 values (meaning all the variables measured in the field and *flowlength*), comparisons among two groups were done with  $t$  tests and comparisons among the three groups with one-way ANOVA with Bonferroni adjustments of  $P$ -values.

For all the spatial metrics for which there are three replicates per site (because of the three images), we used linear regressions to test the trends of the spatial metrics along the aridity gradient evaluated. To do so, we used a mixed-effect linear model with the site as random effect on the intercept and with either aridity or group (healthier or degraded) as the sole fixed effect. These models were fitted using the R package lme4 v1.1-29 (42). More specifically, for the analysis of the effect of aridity on spatial metrics, for example, the linear mixed model:  $I \sim \text{Aridity} + (1 | \text{site})$  was fitted to the data for each spatial metric,  $I$ . Note that the theoretical predictions provide the expected directions of change in the spatial metrics along a stress gradient (i.e., increase or decrease). The significance of the fixed effect (either aridity or group) was tested by likelihood ratio test between the full model (with the fixed and the random effect) and a model without the fixed effect (i.e., with only the random effect).

The slope coefficient estimated for the fixed effect in this linear model indicates how the spatial metrics (observed or null) change along the aridity gradient (a positive slope means that the metric increases with aridity). To make the slopes easier to compare across indicators and to be represented in figures, we standardized the observed and null indicator values. We computed the mean and SD of all observed and null values taken together, then subtracted this mean to both the observed and null values, and divided by the SD, obtaining a standardized effect size. This yielded slopes that are within the same order of magnitude for all indicators, while still allowing the comparison of observed and null slopes for a given indicator.

To obtain CI on the slope estimates (and thus test significant departure from zero), we used ordinary bootstrap in which the slope was reestimated based on 2,999 resampling with replacement of the data used to carry out the fit. To determine CI using bootstrapping, we need a high number of resamples so that the tails of the resulting distribution of slopes are well-sampled; we used  $\text{BOOTN} = 2,999$  based on recommendations in the literature (51).

The *flowlength* metric had only one value per site, thus it did not require the use of mixed-effect modeling—for this spatial metric, we used a simple linear model but did use bootstrap to get CI on the slope.

**Spatial Models of Dryland Vegetation Dynamics.** We ran simulations from two mathematical models of the spatiotemporal dynamics of vegetation in dryland ecosystems. Only the results of Model 1 are displayed in the main text, while the results of Model 2 are in *SI Appendix, section E*.

Model 1 (Kéfi et al. ref. 2). We simulated the spatiotemporal dynamics of a dryland ecosystem using a stochastic cellular automaton model that produces spatial structure of the vegetation like the one observed in empirical data (2, 5, 13, 22–24). In this model, an ecosystem is represented by a grid of cells, each of which can be in one of three states: vegetated, empty, or degraded (2). Empty cells represent fertile soil, whereas degraded cells represented eroded soil locations that are unsuitable for recolonization by vegetation. A key ecological mechanism is local facilitation, i.e., the positive effect of vegetation on its local neighborhood through increased regeneration of degraded cells. Because of this local facilitation, vegetated cells tend to form patches, i.e., sets of vegetated cells connected by a shared edge (von Neumann neighbors, i.e., the four nearest neighbors). When aridity increases, there is a point at which the vegetation dies out and the system becomes a desert through a saddle-node (or fold) bifurcation. The model exhibits bistability for a range of aridity values (parameter  $1-b$  in the model, see *SI Appendix, section A* for a detailed model description), with the coexistence of a vegetated and a desert state (13). To evaluate the effect of the facilitation mechanism on the trends in spatial metrics observed, we also ran simulations without the facilitation mechanism. A more detailed description of the model as well as the parameter values used are available in *SI Appendix, section A*.

Model 2 (Scanlon et al. ref. 8). We checked whether the results we obtained were similar in a second model (8), which is also a cellular automaton but considers only two possible states for the cells, namely trees and empty. The probability of establishment of new trees is assumed to increase with the neighborhood tree density, where the effect of the neighborhood tree density is a weighted as a function of the distance to the focal cell. Conversely, the probability of tree mortality increases with more empty cells in the neighborhood of a given tree. The model description, parameter values are in *SI Appendix, section A* and the results in *SI Appendix, section E* and Figs. S8 and S9.

**Simulations of the Two Models.** We ran simulations on lattices of  $100 \times 100$  cells. For each aridity level, we recorded the final landscape after 10,000 timesteps (for which steady state in overall cover was typically reached). All spatial metrics and their corresponding null values were computed on these landscapes (transformed into matrices of presence/absence of vegetation, i.e., removing information about whether empty sites are fertile or degraded for Model 1) in exactly the same way as previously explained for the data.

**Data, Materials, and Software Availability.** Field data and code data have been deposited in [https://github.com/skefi/spatialaws\\_biocom](https://github.com/skefi/spatialaws_biocom) (52).

**ACKNOWLEDGMENTS.** S.K. was supported by the Alexander von Humboldt foundation. This research was supported by the European Research Council [ERC Grant Agreements 242658 (BIOCOM) and 647038 (BIODESERT)] and Generalitat Valenciana (CIDEGENT/2018/041). F.T.M. acknowledges the support from the University of Alicante (UADIF22-74 and VIGROB22-350) and the Spanish Ministry of Science and Innovation (PID2020-116578RB-I00). A.G. has received funding from the European Union's Horizon 2020 research and innovation programme under the Marie Skłodowska-Curie grant agreement no. 896159. M.B. acknowledges the funding from Spanish Ministry of Science and Innovation through a Ramón y Cajal Fellowship (#RYC2021-031797-I). E.G. acknowledges the support by the Generalitat Valenciana and European Social Fund grant APOSTD/2021/188.

Author affiliations: <sup>a</sup>Institut des Sciences de l'Evolution de Montpellier (ISEM), CNRS, Univ. de Montpellier, Institut de recherche pour le développement (IRD), Montpellier 34095, France; <sup>b</sup>Santa Fe Institute, Santa Fe, NM 87501; <sup>c</sup>Ecosystem Modeling Group, Center for Computational and Theoretical Biology, University of Würzburg, Würzburg, Germany; <sup>d</sup>Environmental Sciences, Copernicus Institute of Sustainable Development, Utrecht University, Utrecht 3508TC, The Netherlands; <sup>e</sup>Estación Costera de Investigaciones Marinas, Pontificia Universidad Católica de Chile, Las Cruces 2690000, Chile; <sup>f</sup>Department of Biodiversity, Ecology and Evolution, Faculty of Biology, Complutense University of Madrid, Madrid 28040, Spain; <sup>g</sup>Instituto Multidisciplinar para el Estudio del Medio "Ramón Margalef," Universidad de Alicante, Alicante 03690, Spain; <sup>h</sup>School of Biosciences, College of Life and Environmental Sciences, University of Birmingham, Birmingham B15 2TT, United Kingdom; <sup>i</sup>Centre d'Ecologie et des Sciences de la Conservation (CESCO), MNHN, CNRS, Sorbonne Univ., 75005 Paris, France; <sup>j</sup>Catalan Institution for Research and Advanced Studies-Complex Systems Lab, Universitat Pompeu Fabra, Barcelona 08003, Spain; <sup>k</sup>Institute of Evolutionary Biology, Spanish National Research Council (CSIC)-Universitat Pompeu Fabra, Barcelona 08003, Spain; and <sup>l</sup>Departamento de Ecología, Universidad de Alicante, Alicante 03690, Spain



1. R. Solé, S. Levin, Ecological complexity and the biosphere: The next 30 years. *Philos. Trans. R. Soc. B Biol. Sci.* **377**, 20210376 (2022).
2. S. Kéfi *et al.*, Spatial vegetation patterns and imminent desertification in Mediterranean arid ecosystems. *Nature* **449**, 213–217 (2007).
3. M. Rietkerk, S. C. Dekker, P. C. de Ruiter, J. van de Koppel, Self-organized patchiness and catastrophic shifts in ecosystems. *Science* **305**, 1926–1929 (2004).
4. M. Rietkerk *et al.*, Evasion of tipping in complex systems through spatial pattern formation. *Science* **374**, eabj0359 (2021).
5. S. Kéfi *et al.*, Early warning signals of ecological transitions: Methods for spatial patterns. *PLoS One* **9**, e92097 (2014).
6. J. van de Koppel *et al.*, Experimental evidence for spatial self-organization and its emergent effects in mussel bed ecosystems. *Science* **322**, 739–742 (2008).
7. M. R. Aguiar, O. E. Sala, Patch structure, dynamics and implications for the functioning of arid ecosystems. *Trends Ecol. Evol.* **14**, 273–277 (1999).
8. T. M. Scanlon, K. K. Caylor, S. A. Levin, I. Rodríguez-Iturbe, Positive feedbacks promote power-law clustering of Kalahari vegetation. *Nature* **449**, 209–212 (2007).
9. N. Barbier, P. Couteron, J. Lejoly, V. Deblauwe, O. Lejeune, Self-organized vegetation patterning as a fingerprint of climate and human impact on semi-arid ecosystems. *J. Ecol.* **94**, 537–547 (2006).
10. V. Deblauwe, N. Barbier, P. Couteron, O. Lejeune, J. Bogaert, The global biogeography of semi-arid periodic vegetation patterns. *Glob. Ecol. Biogeogr.* **17**, 715–723 (2008).
11. J. von Hardenberg, E. Meron, M. Shachak, Y. Zarmi, Diversity of vegetation patterns and desertification. *Phys. Rev. Lett.* **87**, 198101 (2001).
12. C. A. Klausmeier, Regular and irregular patterns in semiarid vegetation. *Science* **284**, 1826–1828 (1999).
13. S. Kéfi, M. Rietkerk, M. van Baalen, M. Loreau, Local facilitation, bistability and transitions in arid ecosystems. *Theor. Population Biol.* **71**, 367–379 (2007).
14. Á. G. Mayor, S. Bautista, E. E. Small, M. Dixon, J. Bellot, Measurement of the connectivity of runoff source areas as determined by vegetation pattern and topography: A tool for assessing potential water and soil losses in drylands - Mayor - 2008 - Water Resources Research - Wiley Online Library. *Water Resources Res.* **44**, W10423 (2008).
15. C. Wissel, A universal law of the characteristic return time near thresholds. *Oecologia* **65**, 101–107 (1984).
16. L. Dai, K. S. Korolev, J. Gore, Slower recovery in space before collapse of connected populations. *Nature* **496**, 355–358 (2013).
17. M. Scheffer *et al.*, Early-warning signals for critical transitions. *Nature* **461**, 53–59 (2009).
18. S. Eby *et al.*, Alternative stable states and spatial indicators of critical slowing down along a spatial gradient in a savanna ecosystem. *Glob. Ecol. Biogeogr.* **26**, 638–649 (2017).
19. L. Rindi, M. Dal Bello, L. Benedetti-Cecchi, Experimental evidence of spatial signatures of approaching regime shifts in macroalgal canopies. *Ecology* **99**, 1709–1715 (2018).
20. M. Berdugo, S. Kéfi, S. Soliveres, F. T. Maestre, Plant spatial patterns identify alternative ecosystem multifunctionality states in global drylands. *Nat. Ecol. Evol.* **1**, 0003 (2017).
21. F. T. Maestre *et al.*, Plant species richness and ecosystem multifunctionality in global drylands. *Science* **335**, 214 (2012).
22. S. Kéfi *et al.*, Robust scaling in ecosystems and the meltdown of patch size distributions before extinction. *Ecol. Lett.* **14**, 29–35 (2011).
23. F. D. Schneider, S. Kéfi, Spatially heterogeneous pressure raises risk of catastrophic shifts. *Theor. Ecol.* **9**, 207–217 (2016).
24. Á. G. Mayor *et al.*, Feedbacks between vegetation pattern and resource loss dramatically decrease ecosystem resilience and restoration potential in a simple dryland model. *Landscape Ecol.* **28**, 931–942 (2013).
25. A. G. Mayor, S. Bautista, F. Rodríguez, S. Kéfi, Connectivity-mediated ecohydrological feedbacks and regime shifts in drylands. *Ecosystems* **22**, 1497–1511 (2019).
26. I. Rodríguez-Iturbe, Z. Chen, A. C. Staver, S. A. Levin, Tree clusters in savannas result from islands of soil moisture. *Proc. Natl. Acad. Sci. U.S.A.* **116**, 6679–6683 (2019).
27. M. Berdugo *et al.*, Global ecosystem thresholds driven by aridity. *Science* **367**, 787–790 (2020).
28. J. M. Yeomans, J. M. Yeomans, *Statistical Mechanics of Phase Transitions* (Oxford University Press, 1992).
29. Rodríguez-Iturbe I., Rinaldo A., *Fractal River Basins, Hydrology, Hydrogeology and Water Resources* (Cambridge University Press, 2001), 16 August 2023.
30. O. Artime, M. De Domenico, From the origin of life to pandemics: Emergent phenomena in complex systems. *Philos. Trans. R Soc A Math. Phys. Eng. Sci.* **380**, 20200410 (2022).
31. A. C. Staver, G. P. Asner, I. Rodríguez-Iturbe, S. A. Levin, I. P. J. Smit, Spatial patterning among savanna trees in high-resolution, spatially extensive data. *Proc. Natl. Acad. Sci. U.S.A.* **116**, 10681–10685 (2019).
32. C. S. Holling, Resilience and stability of ecological systems. *Ann. Rev. Ecol. Syst.* **4**, 1–23 (1973).
33. S. Sankaran, S. Majumder, A. Viswanathan, V. Guttal, Clustering and correlations: Inferring resilience from spatial patterns in ecosystems. *Methods Ecol. Evol.* **10**, 2079–2089 (2019).
34. G. R. Onatibia, L. Boyero, M. R. Aguiar, Regional productivity mediates the effects of grazing disturbance on plant cover and patch-size distribution in arid and semi-arid communities. *Oikos* **127**, 1205–1215 (2018).
35. A. Génin *et al.*, Spatially heterogeneous stressors can alter the performance of indicators of regime shifts. *Ecol. Indicators* **94**, 520–533 (2018).
36. C. Boettiger, A. Hastings, From patterns to predictions. *Nature* **493**, 157–158 (2013).
37. R. Zomer, A. Trabucco, O. van Straaten, D. Bossio, *Carbon, Land and Water: A Global Analysis of the Hydrologic Dimensions of Climate Change Mitigation through Afforestation/Reforestation* (International Water Management Institute, 2006), 4 October 2020.
38. R. J. Hijmans, S. E. Cameron, J. L. Parra, P. G. Jones, A. Jarvis, Very high resolution interpolated climate surfaces for global land areas. *Int. J. Climatol.* **25**, 1965–1978 (2005).
39. M. Delgado-Baquerizo *et al.*, Decoupling of soil nutrient cycles as a function of aridity in global drylands. *Nature* **502**, 672–676 (2013).
40. C. J. Tucker, C. Vanpraet, E. Boerwinkel, A. Gaston, Satellite remote sensing of total dry matter production in the Senegalese Sahel. *Remote Sensing Environ.* **13**, 461–474 (1983).
41. A. Génin *et al.*, Monitoring ecosystem degradation using spatial data and the R package *spatialwarnings*. *Methods Ecol. Evol.* **9**, 2067–2075 (2018).
42. R Core Team, *R: A Language and Environment for Statistical Computing* (R Foundation for Statistical Computing, Vienna, Austria, 2022).
43. V. Guttal, C. Jayaprakash, Spatial variance and spatial skewness: Leading indicators of regime shifts in spatial ecological systems. *Theor. Ecol.* **2**, 3–12 (2009).
44. V. Dakos, E. H. van Nes, R. Donangelo, H. Fort, M. Scheffer, Spatial correlation as leading indicator of catastrophic shifts. *Theor. Ecol.* **3**, 163–174 (2010).
45. S. Sankaran, S. Majumder, S. Kéfi, V. Guttal, Implications of being discrete and spatial for detecting early warning signals of regime shifts. *Ecol. Indicators* **94**, 503–511 (2018).
46. K. R. Clarke, P. J. Somerfield, R. N. Gorley, Testing of null hypotheses in exploratory community analyses: Similarity profiles and biota-environment linkage. *J. Exp. Marine Biol. Ecol.* **366**, 56–69 (2008).
47. L. Scrucca, M. Fop, T. B. Murphy, A. E. Raftery, mclust 5: Clustering, classification and density estimation using Gaussian Finite mixture models. *R J* **8**, 289–317 (2016).
48. M. Hirota, M. Holmgren, E. H. Van Nes, M. Scheffer, Global resilience of tropical forest and savanna to critical transitions. *Science* **334**, 232–235 (2011).
49. M. Scheffer, M. Hirota, M. Holmgren, E. H. Van Nes, F. S. Chapin, Thresholds for boreal biome transitions. *Proc. Natl. Acad. Sci. U.S.A.* **109**, 21384–21389 (2012).
50. V. N. Livina, F. Kwasiok, T. M. Lenton, Potential analysis reveals changing number of climate states during the last 60 kyr. *Clim. Past* **6**, 77–82 (2010).
51. T. J. DiCiccio, B. Efron, Bootstrap confidence intervals. *Stat. Sci.* **11**, 189–228 (1996).
52. S. Kéfi, A. Génin, Code associated with the paper 'Dryland resilience to aridity is associated with self-organized vegetation patchiness'. GitHub: [https://github.com/skefi/spatialawls\\_biocom](https://github.com/skefi/spatialawls_biocom). Deposited 5 February 2023.